

# 2023 年臺灣國際科學展覽會 優勝作品專輯

作品編號 100043

參展科別 工程學

作品名稱 **An Efficient and Accurate  
Super-Resolution Approach to Low-Field  
MRI via U-Net Architecture With  
Logarithmic Loss and L2 Regularization**

得獎獎項

國家 **United States**

就讀學校 **Hartford Union High School**

指導教師

作者姓名 **Aryan Kalluvila**

關鍵詞 **LF-MRI—low-field magnetic resonance  
images、SISR—single image super-resolution、  
CNN—convolutional neural network**

**Abstract:** Low-field (LF) MRI scanners have the power to revolutionize medical imaging by providing a portable and cheaper alternative to high-field MRI scanners. However, such scanners are usually significantly noisier and lower quality than their high-field counterparts. This prevents them from appealing to global markets. The aim of this paper is to improve the SNR and overall image quality of low-field MRI scans (called super-resolution) to improve diagnostic capability and, as a result, make it more accessible. To address this issue, we propose a Nested U-Net neural network architecture super-resolution algorithm that outperforms previously suggested super-resolution deep learning methods with an average PSNR of  $78.83 \pm 0.01$  and SSIM of  $0.9551 \pm 0.01$ . Our ANOVA paired t-test and Post-Hoc Tukey test demonstrate significance with a p-value  $< 0.0001$  and no other network demonstrating significance higher than 0.1. We tested our network on artificial noisy downsampled synthetic data from 1500 T1 weighted MRI images through the dataset called the T1-mix. Four board-certified radiologists scored 25 images (100 image ratings total) on the Likert scale (1-5) assessing overall image quality, anatomical structure, and diagnostic confidence across our architecture and other published works (SR DenseNet, Generator Block, SRCNN, etc.). Our algorithm outperformed all other works with the highest MOS,  $4.4 \pm 0.3$ . We also introduce a new type of loss function called natural log mean squared error (NLMSE), outperforming MSE, MAE, and MSLE on this specific SR task. Additionally, we ran inference on actual Hyperfine scan images with successful qualitative results using a Generator RRDB block. In conclusion, we present a more accurate deep learning method for single image super-resolution applied to low-field MRI via a Nested U-Net architecture.

---

## Introduction

Magnetic resonance imaging (MRI) has revolutionized healthcare by providing a non-invasive diagnostic tool that can output high-resolution images of various anatomical structures. Although traditional MRI scanners operating at high magnetic field strengths (1.5T-3T) provide high sub-millimeter resolution scans, it is very cost-prohibitive and time-intensive due to the high magnetic field strength, installation costs, and operation of the machinery. As of 2021, there are approximately seven high-field MRI scanners per million inhabitants, and over 90% of such scanners are concentrated in high-income countries [3]. In 2020, the FDA approved the world's first portable low-field (LF) human MRI scanner that operates at a significantly lower magnetic field strength (of 64 mT) - the Hyperfine® scanner. Apart from being the most affordable scanners worldwide, specially to developing countries (around \$50K/scanner) [4], LF scanners have enabled ICU patient scanning at bedside while being surrounded by ventilators and other metallic medical devices. However, lowering the magnetic field strength comes with its own challenges. Mainly, there is a significant drop in the signal-to-noise ratio (SNR) and overall image quality. In this paper, we focus on increasing the SNR and resolution of synthetic LF MRI scans via a Nested U-Net deep learning architecture. This neural network architecture has the base U-Net as the blueprint but utilizes redesigned skip connections [18].

While high-field (HF) MRI scanners provide high resolution (HR) to display anatomical structures, which is a requisite for diagnosis of many pathologies such as multiple sclerosis, smaller brain injuries, and neurocognitive diseases (Alzheimer's, Parkinson's), there are medical specialties like emergency medicine where high resolution scans are not an immediate necessity and are therefore not cost-effective for local hospitals and clinics. Instead, a portable LF MRI scanner can be more appealing to such institutions provided the scanners output high enough spatial resolution and with sufficient diagnostic capabilities. One option for approaching this is improving the reconstruction method from the k-space to the image domain, however, this has only limited SNR improvement as k-space has very limited data input [5]. Another option would be to increase the low-field MRI acquisition time and magnetic strength; however, this makes the scan longer for the patient and makes it less suitable for portable bedside imaging [6].

Among the super-resolution (SR) deep learning approaches used to improve spatial resolution of images, single image super-resolution (SISR) has the capability to improve

the SNR and overall image quality without altering any physical MRI properties. Previously, substantial work has been done on 3D low-field MRI super-resolution (or multi-image super-resolution (MISR)) [7]. In this paper, we focus on SISR because it requires less computational power and usually reports higher accuracy (due to greater dataset availability). Furthermore, very often radiologists analyze 2D MRI images to make a diagnosis, especially in emergency situations. 3D scans, even though they provide more information, take a great amount of time to analyze. In that way, 2D LF MRI SISR is more appropriate for emergency care imaging.

Current state-of-the-art SR methods involve three types of methods: interpolation-based, reconstruction-based, and learning-based techniques with the first two being analytical reconstruction methods, and the last one being a machine learning based approach [8-10]. Bilinear/bicubic interpolation techniques, while very computationally efficient, tend to over-smooth and provide granulated outputs, and tend to report small SNR improvements [11]. Reconstruction-based methods solve the blurred edges and granulation produced by interpolation by using a gradient and spatial extraction approach but lack finer details [9]. Learning-based techniques often utilize machine learning to bridge the resolution gap. These techniques report the highest SNR and overall image quality because they usually learn from a large dataset of paired degraded and HR images [10]. Andrew et al. reported using a lightweight autoencoder that leverages skip connections to sufficiently super-resolve downsampled high resolution MRI data [12]. M.L. de Leeuw den Bouter et al. trained an SR DenseNet and were able to inference on a low-field MRI scan to bridge the resolution gap [1]. Laguna et al. implemented a pipeline involving a domain adaptation network, a denoiser, and an SR block to adequately super-resolve 3D MRI scans [13]. The authors' network involved a Residual Dense Block in the SRGAN generator to reconstruct LF MR images. Their work is focused on the domain adaptation portion of the network as bridging the gap between the low-field image domain and the high-field image domain, which is quite difficult. For simplicity, we assume domain adaptation will be sufficiently close to high-field MRI data so that our SR block can reconstruct properly. In this paper, we propose using a SR U-Net++ architecture (Nested U-Net) to reconstruct HR images from synthetically downsampled LF images. We trained the network to output the difference between the high-field and synthetic low-field data as shown in Figure 2. We compared our technique to state-of-the-art methods that included SRCNN, VDSR, and a variation of the SRGAN generator [13].

The major contributions of this work are as follows:

- A down sampling pipeline that accurately transfers HF MRI images to LF MRI images.
- A trained U-Net++ architecture for synthetic LF MRI scans to achieve SISR through employing residual learning
- Comparison of the U-Net++ architecture against state-of-the-art algorithms to evaluate performance through PSNR, SSIM, and a board-certified radiologist
- Evaluation of a varied network on Hyperfine scanners with rigorous domain adaptation and data augmentation

## 2. Materials and Methods

### 2.1 Dataset Preparation

In this study, a total of 1,500 T1-weighted 3T MR human brain images and 20 Hyperfine scans were used. The datasets were primarily the 1,500 3T scans from the T1-Mix dataset. The T1-Mix dataset contained a mix of the following datasets: ABIDE (Di Martino et al., 2014), ADHD200 (Consortium, 2012), GSP (Holmes et al., 2015), HABS (Dagley et al., 2017), MCIC (Gollub et al., 2013), OASIS (Marcus et al., 2007), and PPMI (Marek et al., 2011). Though all the brain images in the training set had a T1-weighted contrast, there were various head positionings and different sequence parameters (like slice thickness). These differences within the training dataset made our U-Net more robust to different types of T1 scans. We then classified T1-Mix as Dataset I. Additionally, all the scans in Dataset I are in the coronal view. The different datasets listed above contained various disorders (such as epilepsy, ADHD, Alzheimer’s, Parkinson’s, autism) but no pathological lesions were included, contributing to the robustness of our U-Net++ trained model.

All 1,500 MRI scans were acquired using a GE 3T MR750 scanner with an 8-channel head coil at the UCSD Center for Functional MRI [14]. The HR scan sequences were acquired from FSPGR T1-weighted sequence (TR: 11.08ms; TE: 4.3ms; flip angle: 45°; FOV: 256mm; 256 x 256 matrix; 180 slices; 1mm<sup>3</sup> in-plane resolution) [14]. Foam pillows were put around the patients’ heads to minimize movement [14].

20 low-field MRI inference scans were acquired from a 64 mT Hyperfine Swoop scanner for a separate segmentation study from Yale Medical School (. A 100 total 3D scans were taken for that study, however, only 20 of these scans didn’t present any significant

lesions or brain alterations (T1, D:  $12 \times 138 \times 36$ , T1, ND:  $138 \times 112 \times 36$ , T2 AXI, ND:  $112 \times 136 \times 36$ , T2 AXI, D:  $120 \times 146 \times 36$ , FLAIR:  $102 \times 122 \times 36$ ).

## 2.2 Implementation Details

All our training experiments were carried out with 2 datasets: T1-mix and ABIDE and in total 1,500 3T High Field MRI scans were used to train our model. The database was split into 3:1 for the training set and the validation set. The synthetic 64 mT LF MRI scans, being the input to the architecture were generated by our downsampling pipeline from the ground truth HF scans. The ground truth were identified as the regular 3T scans ( $256 \times 256$ ) and the residual image (Synthetic LF image – HF image) were used as the corresponding target of the architecture. The main SR algorithm was based on our proposed U-Net++ with VGG blocks and without batch normalization. Both input and output images had only one channel (not RGB) to increase computational efficiency. Six different state-of-the-art algorithms--VDSR, SR-CNN, SR-GAN, DenseNet, SR U-Net, U-Net++-- were trained with the same parameters as specified below and evaluated.

The network was trained with the Adam optimizer with a learning rate of  $1e-4$ . Weight decay or L2 regularization was also employed in the network with a value of  $5e-4$  which helped prevent the network from overfitting. The entire pipeline was trained using PyTorch 1.9.2 with a NVIDIA Quadro RTX 6000 GPU and 24 GB RAM. All 6 neural networks were trained with both the ABIDE and T1-mix, for 60,000 epochs with a batch size of 1 (no batch normalization was employed for consistency and comparison purposes). Each network’s performance was evaluated using the image metrics PSNR and SSIM.

## 2.3 Downsampling and Training Pipeline

Data collection for training an SR network usually requires paired HF and LF scans of the same patient. However, this method involves non-linear distortions, as well as patient registration for a perfect match. Here, to attain LF MRI quality from HF MRI scans, a unique and more efficient downsampling approach was used as described in Figure 2. Usually, scans are downsampled by the same factor vertically and horizontally. However, at LF, the images are distorted in a unique way.

In an empirical manner, applying an asymmetric downsampling factor in the horizontal and vertical directions of 1.5 and 5 respectively resulted in a less distorted

downsampled image compared to a symmetrical downsampled image. We downsample it this way because the low-field MRI T1-Axial resolution is  $120 \times 52 \times 172$ . This accurately reflects low-field MRI. This elongated downsampled MRI scan of 52 pixels  $\times$  172 pixels was then rescaled using the bilinear interpolation to 256 pixels  $\times$  256 pixels resolution to make for an adequate comparison for high-field scans. This final interpolated image was the input to the U-Net++ architecture. This process produced a cleaner and more efficient downsampling method and training pipeline.

---

**Algorithm 1** Super-Resolution Pipeline

---

Data: 2D High-Field MRI scans after standardization

Step (1) **Compression:**

Downsample 256  $\times$  256 scans 1.5 times horizontally and 5 times vertically to output a distorted scan of 52  $\times$  172.

Step (2) **Bilinear Interpolation:**

Resolve scans up to 256  $\times$  256 resolution using bilinear interpolation filling technique (in order to inaccurately improve pixel quality to reflect LF MRI quality).

Step (3) **SR U-Net++**

Input 256  $\times$  256 scans (from step 2) into the U-Net++ with the target being the residual image (difference between HF scan and synthetic LF image).

Step (4) **Final Reconstruction**

Combine output (from step 3) with the output from step 2 to produce HR looking images

---

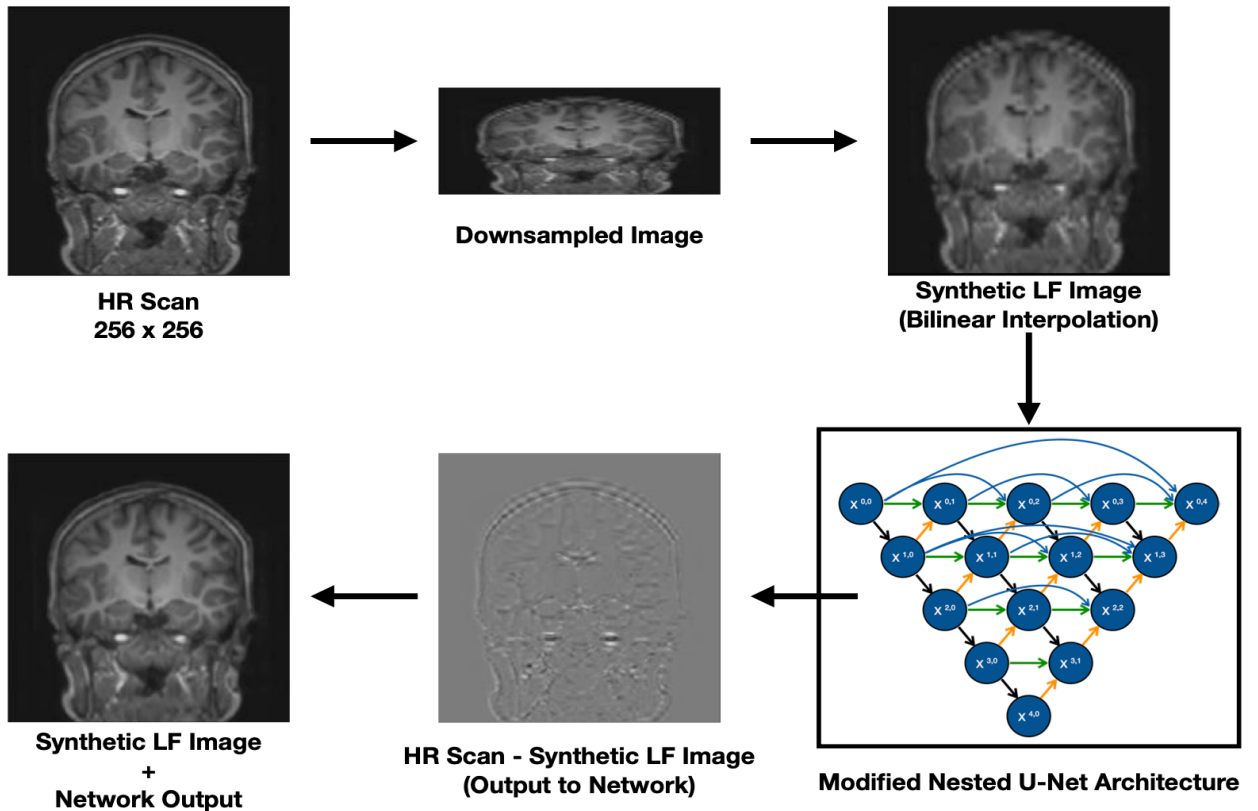


**Figure 1:** SR pipeline network with downsampling process shown, taking a 256  $\times$  256 scan, downsampling it, and applying the U-Net++ algorithm (bottom right).

To improve the performance of the training, all images of the Dataset I were normalized from -0.5 to +0.5. Rigorous data augmentation was performed like random affine, blur, crop, and random rotation, improving the robustness of the neural network and reducing overfitting in the training process. Furthermore, to reduce the computational time, we used a technique called residual learning. As shown in Figure 2 the output/target of the neural network was the difference between the  $256 \times 256$  HF image and the  $256 \times 256$  bilinear interpolated LF image. To reproduce the final SR image, the output was then overlaid onto the bilinear interpolated LF image. This residual learning approach improved the performance of the training since less pixel information is required to be learned by the U-Net++ architecture.

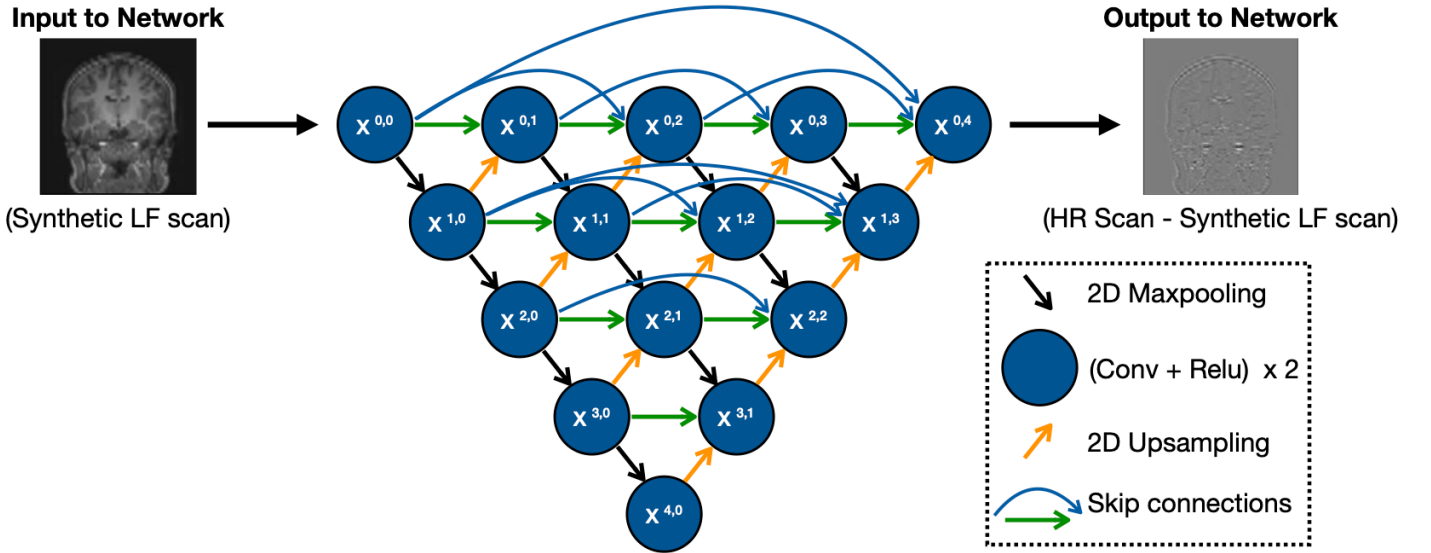


**Figure 2:** Proposed U-Net++ architecture as the primary SR algorithm for this study. This architecture removes the original skip connections as proposed by Zhou Z et al to accurately reconstruct LF MRI images to HF.

#### D. Network Architecture

This section introduces the U-Net++ architecture which is the primary super-resolution algorithm used to reconstruct our synthetic LF brain images. As a well-known architecture in the literature, the standard U-Net involves a symmetric “U” shaped architecture that has a contractive and expansive path (similar to the variational autoencoder). Each downsampling and upsampling layer involves two convolutional layers with padding. The bottom layer (bottleneck) also has two convolutional layers, but no max pooling. Transposed convolutions are used to upsample from the bottleneck layer to the final image size. The benefit of using a U-Net over other architectures is that it is able to localize

and distinguish borders better (due to the classification on each pixel layer) which is suitable for biomedical applications (such as segmentation tasks).

Like the U-Net, the U-Net++ described by Zhou Z et al, involved an encoder and decode to bridge the semantic gap between feature maps prior to diffusion [15]. As shown in Figure 3, the standard U-Net is represented in black circles and the additional skip connections are represented in green and blue dotted arrows. The main distinction between the two networks was the redesigned skip connections (denoted in green and blue dotted arrows). In the standard U-Net, the feature maps of the encoder are directly fed into the decoder, and, our U-Net++ were composed with multiple dense convolutions to improve accuracy of the feature maps before being fed into the decoder. For instance, the skip connection pathway between  $X^{(1,0)}$  to  $X^{(1,3)}$  is composed of three convolutional layers with one dense block where each convolutional layer is preceded by a concatenation layer that fuses the output from the previous convolutional layer [14]

The dense convolutional layers bring the encoder feature maps closer to the decoder feature maps so the accuracy of the overall network is improved. The skip pathway (formulated by Z. Zhou et al.) was created as follows: letting  $x^{(i,j)}$  denote the output node  $X^{(i,j)}$  where  $i$  indexes the down-sampling layer along the encoder and  $j$  indexes the convolutional layer of the dense block along the skip pathway [15]. Z. Zhou et al. also proposed deep supervision on top of the U-Net++ architecture, however, there was no apparent benefit in using deep supervision as that was primarily for segmentation purposes. Instead of using single traditional convolutional layers, visual geometry group blocks (VGGs) were used. VGG blocks are generally composed of multiple convolutional and max pooling layers. Traditional U-Net++ architectures with VGG consist of 1 ReLU activation unit, 2 convolutional layers, and 2 batch normalization layers. Hu et al. proposed a U-Net for image super-resolution without batch normalization and reported a significant increase in overall image quality and resolution [16]. Hence, batch normalization was not used in our proposed U-Net++ architecture as well, improving our architecture by 0.05 in SSIM and 1.34 in PSNR.

### E. Loss Function Customization

In most super-resolution image reconstruction tasks, the loss function employed is the mean squared error loss function as shown in Equation 1,

$$MSE = \frac{1}{n} \sum (Y_i - Y_j)^2 \quad (1)$$

where  $n$  represents total image size,  $Y_i$  represents the output of the network, and  $Y_j$  represents the residual target (synthetic LF – HF). Minimizing such errors produced satisfactory results for random natural images (such as dog, cat, person), but it failed to reconstruct the precise anatomical structures in MRI and CT scans [16]. In this study, we experimented with several different loss functions including: MSE, VGG, and abs-MSE. All of these loss functions produced grainy results, particularly due to the general nature of the functions. Each function can be used for a wide variety of tasks. Thus, we decided to customize our own loss function called Natural Log Mean Squared Error (NLMSE). This function includes a natural log term (or log base  $e$ ) in front of the entire equation and then squares it. In doing so, each pixel is penalized greater, which improves the accuracy of the overall network. Equation 2 outlines our new proposed loss function in comparison to MSE:

$$NLMSE = \frac{1}{n} \log_e (\sum (Y_i - Y_j)^2) \quad (2)$$

## 3. Results

### 3.1 Comparison Against State-of-the-Art Algorithms

To rigorously test the proposed SR U-Net++ architecture, we compared the algorithm against five other state of the art networks which include VDSR, SR-CNN, SR-GAN, DenseNet, SR U-Net. We evaluated all six networks using PSNR and SSIM to get a quantitative evaluation of our networks. We tried to limit our state-of-the-art architectures to SR algorithms that have been applied to MRI super-resolution. Table 2 shows the comparison against state-of-the-art algorithms and the U-Net++ outperforms all networks in terms of both PSNR and SSIM. Comparable to other networks, there isn't marginal improvement. The performance of our proposed network demonstrated the largest increase in PSNR and SSIM performance (+0.29 in PSNR/+0.124 in SSIM).

Table 1: PSNR and SSIM Comparison

Network Type	PSNR	SSIM
Low-Field Scan	75.52	0.9159
VDSR	78.10	0.9481
<b>SR U-Net++ (ours)</b>	<b>78.83</b>	<b>0.9551</b>
SR GAN	75.52	0.9159
SR DenseNet	78.54	0.9519
SR U-Net	78.06	0.9477
SR CNN	78.83	0.9551

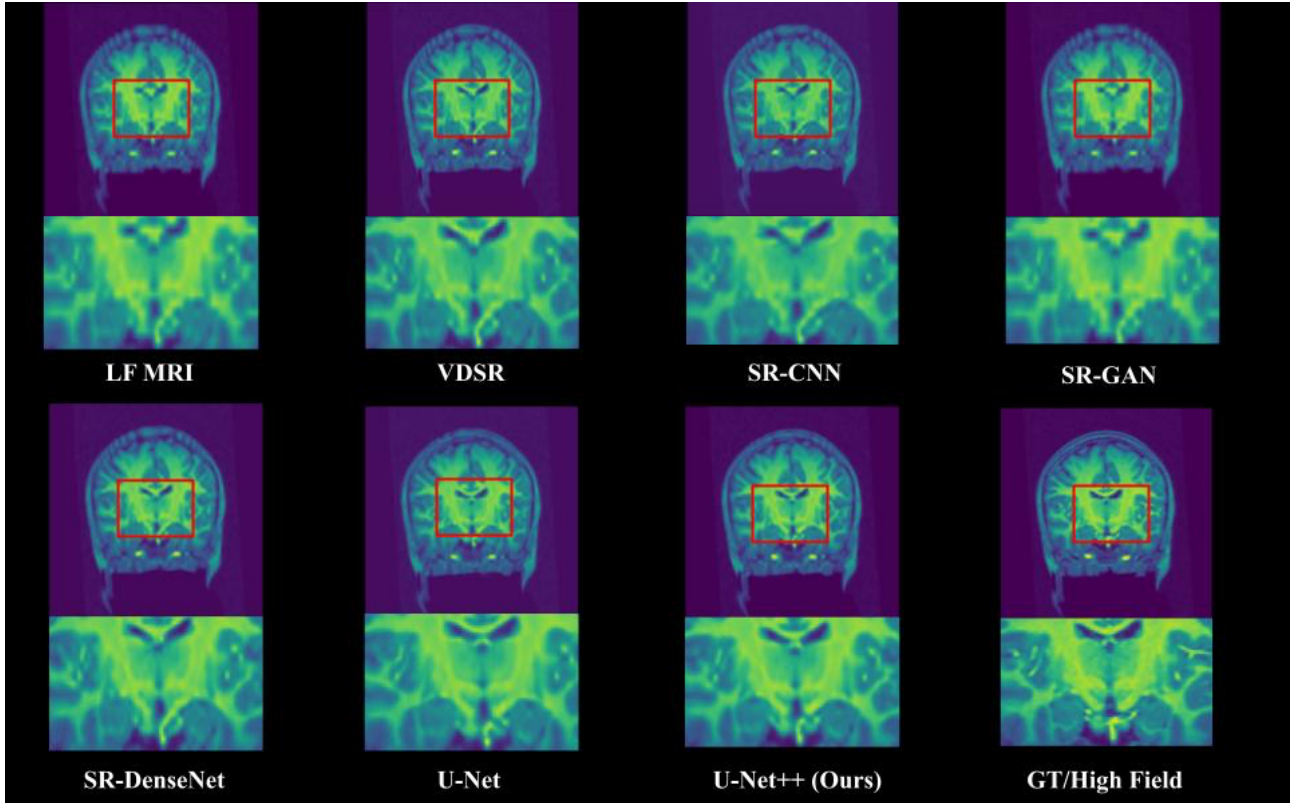


Figure 3: Qualitative observations of LF MRI scans vs super-resolved scans via 5 other networks and the U-Net++ for comparison. The GT/High Field being the reference point.

### 3.2 Mean Opinion Score Testing

Four board-certified radiologists were given 5 scans per network (100 total images) to assess. This was a blinded study where the radiologist had no information on which neural network was used to reconstruct to prevent any bias. The radiologists were asked to rate each subsequent image on a scale from 1-5, with 1 being very close to LF and 5 being very close to HF (the Likert scale). Initially, the radiologist was calibrated by observing 5 LF MRI scans and 5 HF MRI scans to learn the scale. They weren't allowed to

rank in between numbers (such as 3.5). These scores were then averaged and standard deviations were calculated to assess significance ( $F1$  score: 7.037,  $p$ -value: 0.0008)

Table :2 Radiologist Evaluation

Network Type	Mean Opinion Score
Low-Field Scan	$1.0 \pm 0.0$
VDSR	$3 \pm 0.70$
SR CNN	$3.2 \pm 0.44$
SR GAN	$1.0 \pm 0.0$
SR DenseNet	$3.6 \pm 0.55$
SR U-Net	$3.4 \pm 0.89$
<b>SR U-Net++</b>	<b><math>4.4 \pm 0.30</math></b>

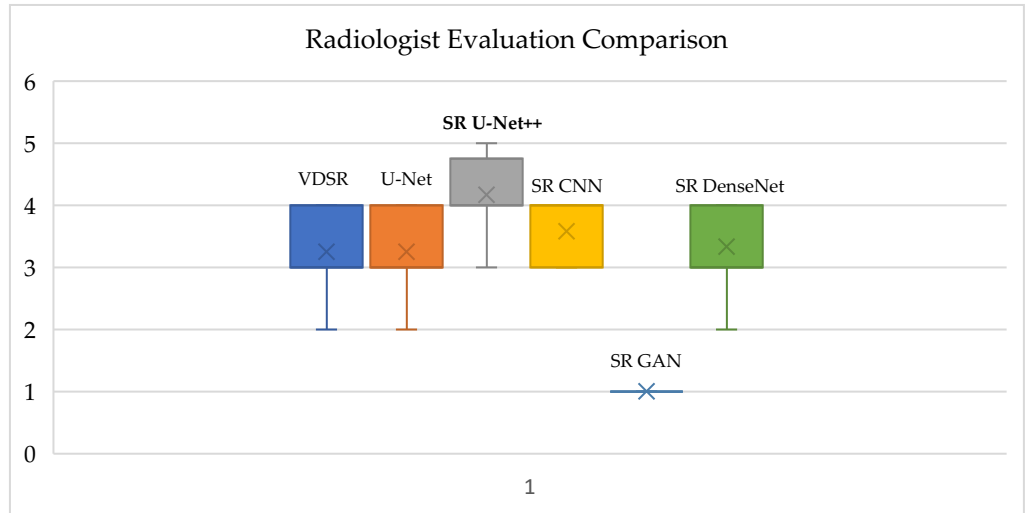


**Figure 4:** A box and whisker plot analysis shows the U-Net++ performing significantly compared to the other networks (even within the confidence interval  $4.4 \pm 0.54$ ). The SR-GAN (blue line with strikethrough) performed the weakest with no deviation (virtually no reconstruction).

The mean opinion score study corroborated well with our PSNR and SSIM studies. In the blind study, all four radiologists chose the U-Net++ architecture as the highest performing network. The U-Net++ outperformed all other networks by at least 0.3 MOS. The radiologist noted improved reconstruction in the hippocampal and skull regions where other networks exhibited artifacting in those regions such as the zebra stripe pattern and bigger hippocampal volume. This study was completed to verify that the U-Net++ reconstructed clinically relevant details. The second best performance was the SR DenseNet proposed by M.L. de Leeuw den Bouter. It is important to note that the SR-GAN had very little reconstruction capabilities, especially with LF MRI super-resolution, potentially due to its volumetric specifications. There was practically no improvement in the the visual or quantitative performance. The synthetic low-field MRI scan was

compared to ground truth when evaluating the PSNR and SSIM which yielded very low values.

### 3.3 Inference on Hyperfine scans

We tested our network on actual low-field MRI scans taken from the Hyperfine scanners. We also altered the network to tailor it Hyperfine scans using a Generator Residual Residual Dense Block (RRDB) block to improve performance, altering the U-Net++. The Generator RRDB block is an alteration of the Generator block used for generative adversarial networks (GANs). Additionally, there was a substantial domain gap which prevented the SR network from producing significant results. To account for this gap, we included a cycleGAN network to bridge the domains and then apply the Generator RRDB block to bridge the resolution.

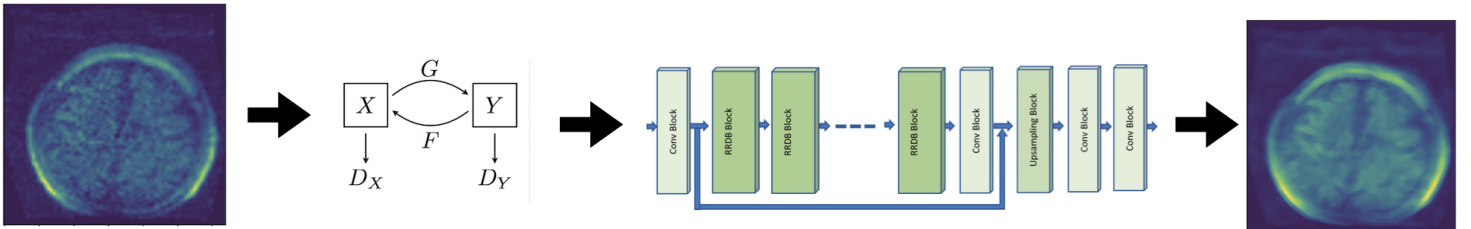


**Figure 5:** Hyperfine super-resolution pipeline. Second portion is the cycleGAN block followed by the Generator RRDB block (U-Net++ alteration) outputting the super-resolved and denoised Hyperfine scan.

The domain adaptation also acted as the denoiser network. Laguna et al proposed a separate denoiser block, however, in our studies, that did not improve the noise issue at all. It caused separate distortions. Without the cycleGAN, all the neural networks tested failed at bridging the gap due to the domain issue.

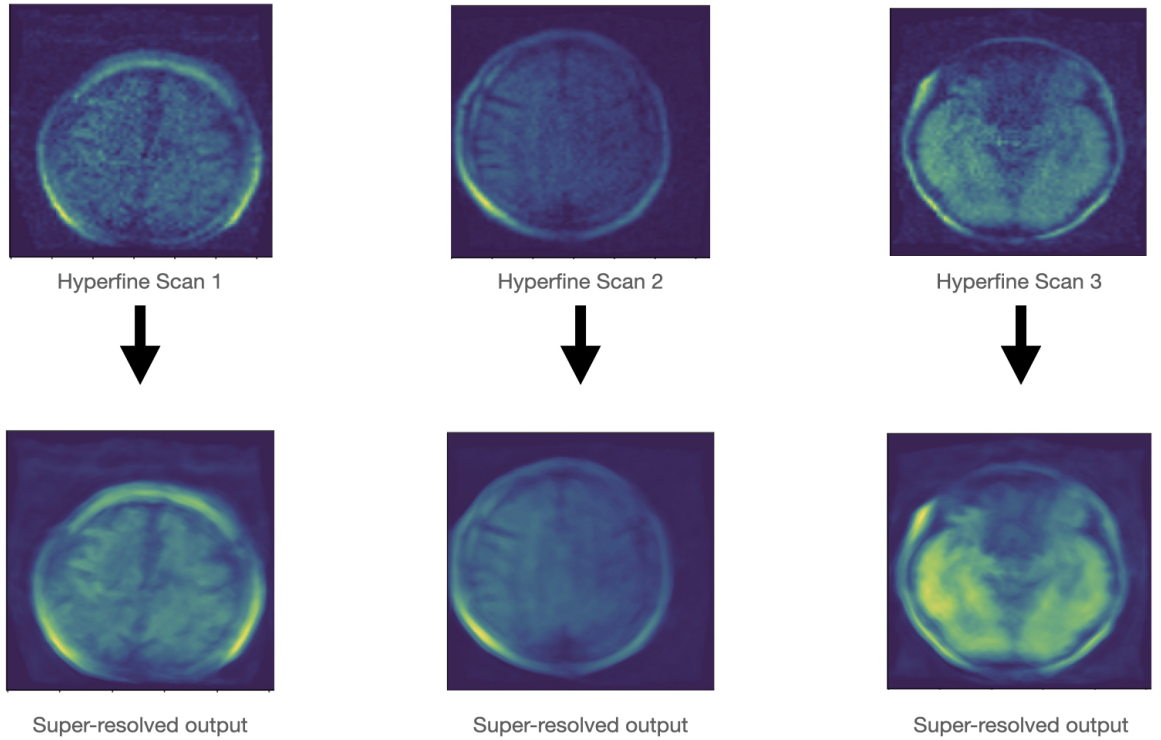


**Figure 6:** Qualitative observations of Hyperfine scans running through the cycleGAN + RRDB block to demonstrate super-resolution significance. Quantitative observations yielded a  $37.01 \pm 4.12$  PSNR and  $0.93 \pm 0.12$ , which improved non-resolved scans by 45%.

#### 4. Discussion

In this study, we demonstrated accurate low-field MRI super-resolution to 3T MRI using a U-Net++ architecture. Our network outperformed current state-of-the-art networks by a substantial amount. This work demonstrates the promise of fully connected U-Nets for medical image super-resolution tasks, especially when filling a larger resolution gap. Previously MRI super-resolution papers aimed to bridge a smaller resolution gap which marginally improves the scanner. However, in this study, we show that a U-Net++ can substantially improve the anatomical resolution of MRI scans with high PSNR and SSIM values.

From Figure 7, there is a substantial improvement in resolution from the other networks and the SR U-Net and SR U-Net++, especially in the inner regions of the brain. The difference between the SR U-Net and the SR U-Net++ is the slight contrast improvement. The redesigned skip connections allow for greater improvement within those areas where the traditional SR U-Net fails. In Table 1, the PSNR and SSIM of the SR U-Net++

outperforms all other state of the art. The U-Net comes in a close second but again hinders due to the contrast difference. A similar SR-DenseNet architecture proposed by M.L. de Leeuw den Bouter was also tested in this study which closed around a 78.08 PSNR and 0.9477 [1]. From Figure 7, this network exhibits some artifacts in the two brain cavities magnified. U-Nets specialize in localization which enables them to smooth out these regions and obtain substantially higher PSNR and SSIM values.

We tested this methodology on actual Hyperfine scans (granted IRB approval). Laguna et. al emphasized the importance of domain adaptation in realistic LF MRI super-resolution as the domain shift turns out to be quite substantial [13]. Our Generator RRDB block and novel cycleGAN improved the quality of the Hyperfine scans substantially (as denoted by Figure 5). Quantitative observations weren't completed as only one method was tested (Generator RRDB block + cycleGAN). These proved to outperform all the other networks visually.

Transformers have seen recent news in NLP and visual machine learning tasks. Applying such algorithms to medical image super-resolution could also yield improvement in results. Future studies could involve concatenation of a strong domain adaptation network, a denoiser, and an SR block (like the one we proposed in this study) to corroborate strong LF MRI super-resolution directly from the scanner itself. Here, we seek to improve one part of that pipeline. Also, although we have extensively applied the SR U-Net++ to brain MRI super-resolution, applying it to other organs at LF (especially cardiac imaging) could show the robustness of the SR U-Net++ even further. Additionally, in machine learning terms, we had a relatively small dataset of approximately 2,000 images. Increasing this dataset and performing rigorous augmentation could potentially improve results.

## 5. Conclusion

In this paper, we propose a SR U-Net++, previously used for medical image segmentation, to the task of medical image super-resolution. Specifically, we apply this to LF MRI SISR. From a dataset of about 2,000 images taken from healthy patients and autistic patients, we create synthetic LF MRI images using a unique downsampling pipeline designed for 64 LF MRI reconstruction. For the primary reconstruction pipeline, we used a U-Net++ which takes on the original U-Net architecture but redesigns the skip connections instead of just directly feeding the features maps from the encoder to the decoder. The skip connections are VGG convolutional blocks stripped of batch normalization to improve decoder

accuracy. We also propose a new SR loss function called NLMSE which improves accuracy substantially. From PSNR and SSIM studies, the U-Net++ outperforms all tested state-of-the-art algorithms. For the qualitative inspection, the U-Net and U-Net++ recover local pixel details at greater detail than any other tested network. The U-Net++ is speculated to have improved contrast, however with a PSNR of 78.83 and SSIM and 0.9551.

We also completed MOS testing to verify the clinic relevance of the reconstructed areas from the U-Net++. In this blind study, the U-Net++ was chosen as the highest performing network. Overall, the U-Net++ is a strong contender for LF MRI super-resolution. We also ran inference on 20 Hyperfine scans using a generator RRDB block and cycleGAN domain adaptation and this proved to yield strong visual results, showing promise for neural networks in future LF MRI super-resolution tasks.

**Author Contributions:** A.K., dataset preprocessing, neural network development, loss function development, statistical analysis, data curation, investigation, formal analysis, writing—original draft preparation. D.B., writing—review and editing., N.K, writing—review and editing, M.Rock, radiologist completing MOS analysis, M.R., supervision, conceptualization, resources, writing—review and editing.

**Funding:** This research received no external funding from other sources.

**Institutional Review Board Statement:** The 20 Hyperfine scans are an approved study from the Institutional Review Board. (Protocol Number: 2020P002952, Process Type: AME24).

**Informed Consent Statement:** Informed consent was obtained from all subjects involved in the study.

**Data Availability Statement:** The T1-mix dataset is a consortium of 7 different datasets which is publicly available at: ABIDE (Di Martino et al., 2014), ADHD200 (Consortium, 2012), GSP (Holmes et al., 2015), HABS (Dagley et al., 2017), MCIC (Gollub et al., 2013), OASIS (Marcus et al., 2007), and PPMI (Marek et al., 2011).

**Acknowledgments:** The authors would like to acknowledge Dr. Juan Eugenio Iglesias and Dr. Sean Young for their contributions with datasets and data preprocessing.

**Conflicts of Interest:** All the authors declare no conflict of interest.

## References

1. de Leeuw den Bouter, M.L., Ippolito, G., O'Reilly, T.P.A. et al. Deep learning-based single image super-resolution for low-field MR brain images. *Sci Rep* 12, 6362 (2022). <https://doi.org/10.1038/s41598-022-10298-6> Author 1, A.; Author 2, B. Title of the chapter. In *Book Title*, 2nd ed.; Editor 1, A., Editor 2, B., Eds.; Publisher: Publisher Location, Country, 2007; Volume 3, pp. 154–196.
2. J. Clerk Maxwell, *A Treatise on Electricity and Magnetism*, 3rd ed., vol. 2. Oxford: Clarendon, 1892, pp.68–73. Author 1, A.B.; Author 2, C. Title of Unpublished Work. *Abbreviated Journal Name* year, phrase indicating stage of publication (submitted; accepted; in press).
3. Liu, Y., Leong, A.T.L., Zhao, Y. et al. A low-cost and shielding-free ultra-low-field brain MRI scanner. *Nat Commun* 12, 7238 (2021). <https://doi.org/10.1038/s41467-021-27317-1>.
4. Deoni, S.C.L., Medeiros, P., Deoni, A.T. et al. Development of a mobile low-field MRI scanner. *Sci Rep* 12, 5690 (2022). <https://doi.org/10.1038/s41598-022-09760-2> Author 1, A.B. Title of Thesis. Level of Thesis, Degree-Granting University, Location of University, Date of Completion.
5. Koonjoo, N., Zhu, B., Bagnall, G.C. et al. Boosting the signal-to-noise of low-field MRI with deep learning image reconstruction. *Sci Rep* 11, 8248 (2021).
6. Erb-Eigner K, Warmuth C, Taupitz M, Willerding G, Bertelmann E, Asbach P. Impact of magnetic field strength and receiver coil in ocular MRI: a phantom and patient study. *Rofo*. 2013 Sep;185(9):830-7. doi: 10.1055/s-0033-1335796. Epub 2013 Jul 25. PMID: 23888471.
7. Chen, Y., Christodoulou, A. G., Zhou, Z., Shi, F., Xie, Y., & Li, D. (2020). MRI Super-Resolution with GAN and 3D Multi-Level DenseNet: Smaller, Faster, and Better. arXiv. <https://doi.org/10.48550/arXiv.2003.01217>
8. Mahmoudzadeh AP, Kashou NH. Interpolation-based super-resolution reconstruction: effects of slice thickness. *J Med Imaging (Bellingham)*. 2014 Oct;1(3):034007. doi: 10.1117/1.JMI.1.3.034007. Epub 2014 Dec 25. PMID: 26158065; PMCID: PMC4478865.
9. Yang Q, Wang H. Super-resolution reconstruction for a single image based on self-similarity and compressed sensing. *Journal of Algorithms & Computational Technology*. 2018;12(3):234-244. doi:10.1177/1748301818778244
10. M. Sharma, S. Chaudhury and B. Lall, "Deep learning based frameworks for image super-resolution and noise-resilient super-resolution," 2017 International Joint Conference on Neural Networks (IJCNN), 2017, pp. 744-751, doi: 10.1109/IJCNN.2017.7965926.
11. Ledig, C., Theis, L., Huszar, F., Caballero, J., Cunningham, A., Acosta, A., Aitken, A., Tejani, A., Totz, J., Wang, Z., & Shi, W. (2016). Photo-Realistic Single Image Super-Resolution Using a Generative Adversarial Network. arXiv. <https://doi.org/10.48550/arXiv.1609.04802>
12. Andrew J., Mhatesh T., Sebastin R.D., Sagayam K.M., Eunice J., Pomplun M., et al. Super-resolution reconstruction of brain magnetic resonance images via lightweight autoencoder *Informatics in Medicine Unlocked*, 26 (2021), Article 100713, 10.1016/j.imu.2021.100713
13. Laguna S, Iglesias J, Rosen M, et. al. Super resolution of portable low field MRI in realistic scenarios. MIDL conference paper.
14. Cameron Craddock, Yassine Benhajali, Carlton Chu, Francois Chouinard, Alan Evans, András Jakab, Budhachandra Singh Khundrakpam, John David Lewis, Qingyang Li, Michael Milham, Chaogan Yan, Pierre Bellec (2013). *The Neuro Bureau*

Preprocessing Initiative: open sharing of preprocessed neuroimaging data and derivatives. In Neuroinformatics 2013, Stockholm, Sweden.

15. Zhou, Z., Siddiquee, M. M., Tajbakhsh, N., & Liang, J. (2018). UNet++: A Nested U-Net Architecture for Medical Image Segmentation. arXiv. <https://doi.org/10.48550/arXiv.1807.10165>
16. X. Hu, M. A. Naei, A. Wong, M. Lamm and P. Fieguth, "RUNet: A Robust UNet Architecture for Image Super-Resolution," 2019 IEEE/CVF Conference on Computer Vision and Pattern Recognition Workshops (CVPRW), 2019, pp. 505-507, doi: 10.1109/CVPRW.2019.00073.
17. Ghodrati V, Shao J, Bydder M, Zhou Z, Yin W, Nguyen KL, Yang Y, Hu P. MR image reconstruction using deep learning: evaluation of network structure and loss functions. *Quant Imaging Med Surg* 2019;9(9):1516-1527. doi: 10.21037/qims.2019.08.10
18. Ronneberger, O., Fischer, P., & Brox, T. (2015). U-Net: Convolutional Networks for Biomedical Image Segmentation. arXiv. <https://doi.org/10.48550/arXiv.1505.04597>

Supplementary Figures (Not Included in Peer-Review)

<i>Pairwise Comparisons</i>		HSD <sub>.05</sub> = 0.6070 HSD <sub>.01</sub> = 0.7336	Q <sub>.05</sub> = 3.9600    Q <sub>.01</sub> = 4.7862
T <sub>1</sub> :T <sub>2</sub>	M <sub>1</sub> = 3.20 M <sub>2</sub> = 3.27	0.07	Q = 0.44 ( <i>p</i> = .99801)
T <sub>1</sub> :T <sub>3</sub>	M <sub>1</sub> = 3.20 M <sub>3</sub> = 4.20	1.00	Q = 6.52 ( <i>p</i> = .00017)
T <sub>1</sub> :T <sub>4</sub>	M <sub>1</sub> = 3.20 M <sub>4</sub> = 3.67	0.47	Q = 3.04 ( <i>p</i> = .20988)
T <sub>1</sub> :T <sub>5</sub>	M <sub>1</sub> = 3.20 M <sub>5</sub> = 3.40	0.20	Q = 1.30 ( <i>p</i> = .88720)
T <sub>2</sub> :T <sub>3</sub>	M <sub>2</sub> = 3.27 M <sub>3</sub> = 4.20	0.93	Q = 6.09 ( <i>p</i> = .00050)
T <sub>2</sub> :T <sub>4</sub>	M <sub>2</sub> = 3.27 M <sub>4</sub> = 3.67	0.40	Q = 2.61 ( <i>p</i> = .35640)
T <sub>2</sub> :T <sub>5</sub>	M <sub>2</sub> = 3.27 M <sub>5</sub> = 3.40	0.13	Q = 0.87 ( <i>p</i> = .97225)
T <sub>3</sub> :T <sub>4</sub>	M <sub>3</sub> = 4.20 M <sub>4</sub> = 3.67	0.53	Q = 3.48 ( <i>p</i> = .11174)
T <sub>3</sub> :T <sub>5</sub>	M <sub>3</sub> = 4.20 M <sub>5</sub> = 3.40	0.80	Q = 5.22 ( <i>p</i> = .00390)
T <sub>4</sub> :T <sub>5</sub>	M <sub>4</sub> = 3.67 M <sub>5</sub> = 3.40	0.27	Q = 1.74 ( <i>p</i> = .73375)

**Supp. Figure 1:** This shows a ANOVA Post-HOC Tukey Analysis of each network (T1-T5, named sequentially in the figures, T-3 = U-Net++). The U-Net++ didn't present any statistical correlation to any other network (outperformed; *p*-value < 0.001), besides the U-Net architecture (T4, *p*-value 0.111).

## 【評語】 100043

1. The work presents a UNET++ architecture to provide super-resolution of low-field MRI images.
2. The approach appears to achieve some performance improvement in comparison with some existing approaches. More precisely , the proposed work is applied to low field MRI. From a dataset of about 2,000 images taken from healthy patients and autistic patients , Low filed MRI images are synthesized using a downsampling pipeline designed for the purposed of super-resolution reconstruction.
3. Some potential applications are also highlighted in the presentation as the work is collaborated with a celebrated medical school.
4. A fair assessment of the proposed approach is recommended. Also , a framework that describes the acquisition of low-field MRI images , inference of the images based on the proposed method , and suggestions for diagnosis is helpful.